

# The Crucial Role of Charge in Thermoresponsive-Polymer-Assisted Reversible Dis/Assembly of Gold Nanoparticles

Vladimir A. Turek, Sean Cormier, Benjamin Sierra-Martin, Ulrich F. Keyser, Tao Ding,\* and Jeremy J. Baumberg\*

Dynamic control of the spacing between Au nanoparticles using nanoarchitectures incorporating the thermoresponsive polymer poly(*N*-isopropylacrylamide) (PNIPAM) has the capability to induce strong color changes from the plasmon shifts. PNIPAM self-assembles on the surface of Au nanoparticles regardless of its terminal group. However, in many cases, the collapse of this PNIPAM coating at elevated temperatures fails to cause a color change, due to electrostatic and steric repulsion between the Au nanoparticles. Here, it is shown how tuning the charge repulsion between the nanoparticles is crucial to achieve large, reversible shifts of the plasmon resonances. Using  $-\text{NH}_2$  terminal groups of the PNIPAM is most effective, compared with  $-\text{SH}$ ,  $-\text{COOH}$ , and  $-\text{H}$  terminations, due to their synergistic role in citrate stripping and charge neutralization. This detailed understanding of the Au–PNIPAM system is vital to enable temperature-responsive plasmonic systems with large tuning ranges, suitable for applications such as plasmonic actuators, displays, and Raman switches.

(PNIPAM) to tune the plasmonic resonance of AuNPs, either via changes in their separation or their dielectric environment.<sup>[6–12]</sup> Although this field of Au–PNIPAM hybrid system has been growing over the last decade, the understanding of how PNIPAM interacts with AuNPs and how it causes the aggregation of AuNPs remains ambiguous.<sup>[6]</sup> The optical response of the hybrid system is highly sensitive to the AuNP functionalization process as well as the concentrations of the constituent parts.<sup>[13,14]</sup> Previously, we showed such hybrid nanoparticle aggregates form actuating nanotransducers (ANTs) providing large local forces exceeding 10 nN.<sup>[9]</sup> A clear understanding of the persisting questions is thus not only timely for proper design of responsive plasmonic systems, but also

applicable much more generally to polymer-assisted colloidal self-assembly.

Here, we uncover how the local charge of AuNPs imparted by the ligands and environment determines the aggregation of nanoparticles and thus plasmon tunability. Other factors are found to be less important, including the functional groups on the PNIPAM chains and their molecular weight. We use a variety of PNIPAM attachments combined with different background salt concentrations to explore the different behaviors of these composite nanoparticles, both above and below the lower critical solution temperature (LCST) of the PNIPAM (around 32 °C).

## 1. Introduction

Tremendous efforts have been devoted to the assembly of gold nanoparticles (AuNPs) because of their intriguing plasmonic properties for many applications as well as their suitability as a model system to understand the colloidal self-assembly process.<sup>[1–4]</sup> Particularly interesting is reversible self-assembly, which creates multistable nanoconfigurations under different conditions, and provides a potential route toward exploiting colloid lattices for information storage and color switches in sensing and displays.<sup>[5]</sup> A common approach is to use thermoresponsive polymers such as poly(*N*-isopropylacrylamide)

## 2. Results

Initially, we measure dynamic light scattering (DLS) of a range of PNIPAM-coated AuNP aggregates when the PNIPAM is collapsed ( $T > 32$  °C), which reveals the radically different hydrodynamic (DLS) sizes for different PNIPAM terminal groups and ionic strength (Table 1, hot DLS). The core–shell nanoparticle solutions are prepared via a “graft to” method by mixing citrate-stabilized 16 nm homemade AuNPs with PNIPAM polymers (Table 1, cold DLS).<sup>[6]</sup> The polymer chains functionalize the surface of AuNPs enabling reversible tuning of plasmons with cycling temperature. Our intuitive understanding is that PNIPAM–SH should work better than other types of PNIPAM because the stronger binding should give

Dr. V. A. Turek, S. Cormier, Dr. B. Sierra-Martin, Prof. U. F. Keyser,  
Prof. T. Ding, Prof. J. J. Baumberg  
Department of Physics  
Nanophotonics Centre  
Cavendish Laboratory  
JJ Thompson Avenue  
University of Cambridge  
Cambridge CB3 0HE, UK  
E-mail: t.ding@whu.edu.cn; jjb12@cam.ac.uk  
Prof. T. Ding  
Key Laboratory of Artificial Micro- and Nano-structures  
of Ministry of Education of China  
School of Physics and Technology  
Wuhan University  
Wuhan 430072, China

DOI: 10.1002/adom.201701270

**Table 1.** Hydrodynamic diameter from DLS data of ANTs for various functionalized PNIPAM with and without  $50 \times 10^{-3}$  M NaCl.

Sample ( $M_w$ )	Au@PNIPAM with/without NaCl [10 kDa]	Au@PNIPAM-NH <sub>2</sub> with/without NaCl [5.5 kDa]	Au@PNIPAM-SH with/without NaCl [15 kDa] <sup>c)</sup>	Au@PNIPAM-COOH with/without NaCl [5 kDa]
DLS hot <sup>a)</sup> (aggregated)	520/50	460/440	680/150	450/76
DLS cold <sup>a)</sup> (single NPs)	94/50	75/60	120/60	60/40
Plasmon Shift (nm) <sup>b)</sup>	40/2	105/30	42/4	75/3

<sup>a)</sup>Hot data corresponds to 40 °C while cold data is at 25 °C; <sup>b)</sup>Plasmon redshifts (from solution extinction spectra) are measured from the plasmon peak in the hot state; <sup>c)</sup>The molecular weight differences do not influence the plasmon shift significantly (see Section 3.1).

more effective actuation, which is why this is what most previous research groups adopted.<sup>[7,8,13,14]</sup> However, our data show PNIPAM-NH<sub>2</sub> giving the largest spectral redshifts and results in the largest average aggregate sizes. Irrespective of which type of PNIPAM binding is used, adding salt increases both the aggregate sizes and the magnitude of the redshift (Table 1).

### 3. Discussion

To understand this data, we instead hypothesize that it is the inner surface charge of AuNPs that determine their aggregation into close proximity, rather than simple agglomeration (Figure 1). The PNIPAM functions here to squeeze the tethered AuNPs together, bringing them into a final proximity set by the PNIPAM-screened repulsion between the Au-Au surfaces. At the concentrations used here, assuming the particles and the polymers are spaced evenly in the solution, AuNPs are initially  $\approx 600$  nm apart while at  $0.1 \text{ mg mL}^{-1}$ , the 15k PNIPAM molecules are  $\approx 40$  nm apart. Because the hydrodynamic radius of the polymers is also much lower than the AuNPs (for 15 kDa PNIPAM this is  $\approx 2.9$  nm),<sup>[15]</sup> the PNIPAM chains are therefore able to diffuse faster and initial aggregation builds PNIPAM cores which encounter AuNPs that adhere on the outside. However, as discussed below, our results will show that the AuNPs remain mobile and are drawn together inside the PNIPAM.

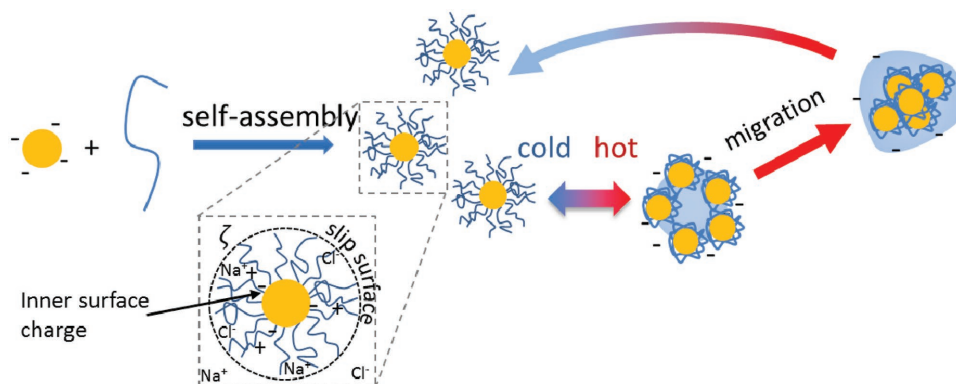


**Figure 1.** Schematic of assembly. Citrate-capped AuNPs bind to short PNIPAM strands (blue) providing steric stabilization when cold (left). The inset (bottom) shows ions inside PNIPAM shell seen with DLS. When heated these core-shell NPs then aggregate as the PNIPAM collapses (right). The AuNPs then travel through the PNIPAM to approach more closely (migration step), depending on the ionic strength and molecular weight of PNIPAM. This assembly is reversible, and is controlled by cycling the temperature of the solution below and above the LCST.

### 3.1. Influence of Different Terminal Groups

The critical dependence on the terminal group of the PNIPAM is particularly puzzling if the overall size of the polymer is considered—it is not intuitive how one functional group in a molecule of  $M_w = 5.5$  kDa (49 polymer units) would radically change the response of the system. To study this in more detail, we compare the extinction spectra of solution-phase aggregates using -NH<sub>2</sub>- and -SH-terminated PNIPAM (Figure 2). As we later show through detailed modeling, larger redshifts of the plasmon peaks are produced for larger clusters and smaller AuNP separations. In the absence of additional salt, triggering the hot state with amine-terminated PNIPAM clearly leads to larger clusters than the thiolated PNIPAM. However when cold, the coated NPs always break apart again into separated nanoparticles (Figure 2d, cold) with each 16 nm AuNP core surrounded by solvated  $\approx 20$  nm PNIPAM strands, giving total diameter of 60 nm. When hot, small aggregates form in the thiolated case but much larger aggregates for amine PNIPAM (as seen directly in Figure 2f). After their collapse, both thiol- and amine-terminated PNIPAM are expected to have similar shell thicknesses, which should give similar separations between the cores and therefore similar redshifts. By calibrating our spectral plasmon ruler (below), the small  $\Delta\lambda = 4$  nm spectral redshifts for the  $D = 150$  nm diameter hot clusters seen with thiolated PNIPAM imply gaps between the NPs of  $d > 30$  nm. We also confirm that the redshift is not significantly affected by the molecular weight as similar redshifts are seen when using thiol-terminated PNIPAM with molecular weight of 5.5 kDa (Figure S1, Supporting Information). By contrast, the  $D = 440$  nm NH<sub>2</sub>-PNIPAM aggregates have redshifts of 30 nm, implying Au-Au gaps around  $d \approx 10$  nm. The termination thus has a profound effect on both the resulting aggregate size as well as the gap between the NPs. This must result from the contrasting interactions between the positively charged amines, the thiols, and the citrate groups on the Au.

duced for larger clusters and smaller AuNP separations. In the absence of additional salt, triggering the hot state with amine-terminated PNIPAM clearly leads to larger clusters than the thiolated PNIPAM. However when cold, the coated NPs always break apart again into separated nanoparticles (Figure 2d, cold) with each 16 nm AuNP core surrounded by solvated  $\approx 20$  nm PNIPAM strands, giving total diameter of 60 nm. When hot, small aggregates form in the thiolated case but much larger aggregates for amine PNIPAM (as seen directly in Figure 2f). After their collapse, both thiol- and amine-terminated PNIPAM are expected to have similar shell thicknesses, which should give similar separations between the cores and therefore similar redshifts. By calibrating our spectral plasmon ruler (below), the small  $\Delta\lambda = 4$  nm spectral redshifts for the  $D = 150$  nm diameter hot clusters seen with thiolated PNIPAM imply gaps between the NPs of  $d > 30$  nm. We also confirm that the redshift is not significantly affected by the molecular weight as similar redshifts are seen when using thiol-terminated PNIPAM with molecular weight of 5.5 kDa (Figure S1, Supporting Information). By contrast, the  $D = 440$  nm NH<sub>2</sub>-PNIPAM aggregates have redshifts of 30 nm, implying Au-Au gaps around  $d \approx 10$  nm. The termination thus has a profound effect on both the resulting aggregate size as well as the gap between the NPs. This must result from the contrasting interactions between the positively charged amines, the thiols, and the citrate groups on the Au.

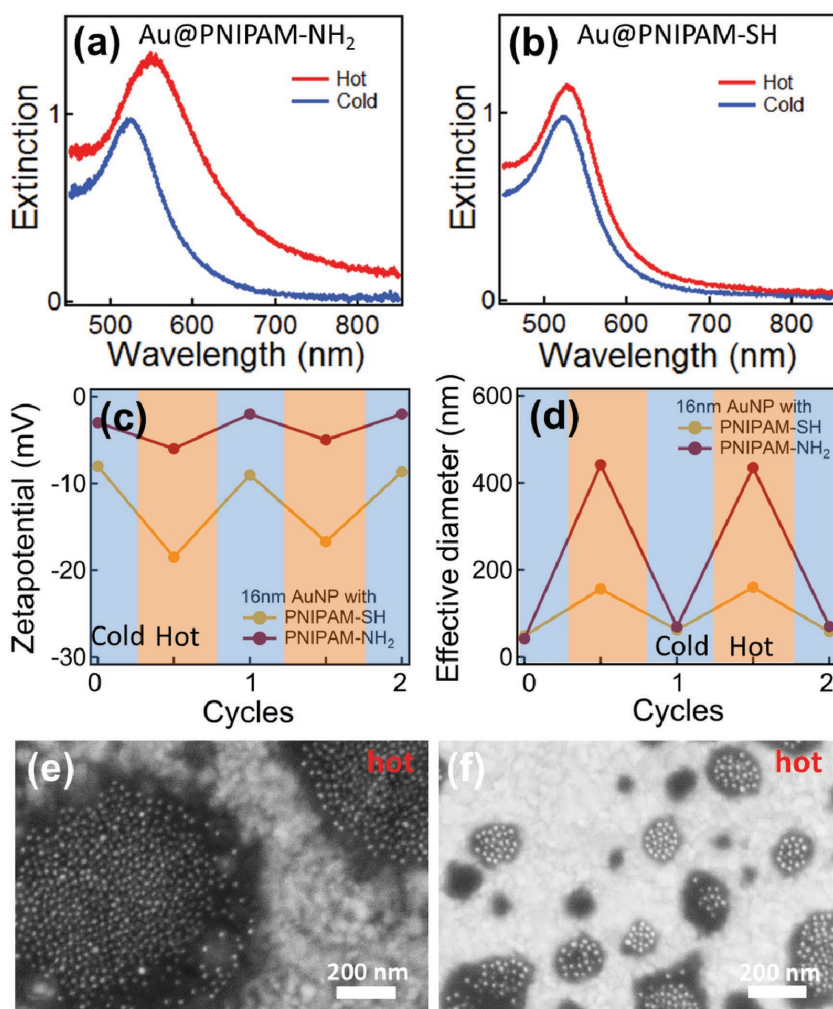


**Figure 2.** a,b) Extinction spectra in solution of PNIPAM-coated 16 nm AuNPs in the hot (45 °C) and cold states (25 °C), using a) amine- and b) thiol-functionalized PNIPAM. c) Zeta-potential measurements reversibly increase in the hot state upon aggregation and d) DLS measurements show larger clusters for  $-\text{NH}_2$  terminated PNIPAM. e,f) SEMs of hot dried aggregates confirm larger clusters for e)  $-\text{NH}_2$  than f)  $-\text{SH}$ -terminated PNIPAM. No extra salt is added.

The zeta-potentials ( $\zeta$ ) of the individual PNIPAM-coated AuNPs include citrate molecules bound to the Au and trapped within the polymer shell, as well as other trapped ions (inset, Figure 1). In the cold state, we find the PNIPAM-coated AuNPs always show a greatly reduced effective charge with  $-\zeta < 10$  mV compared with the initial NPs with  $-\zeta = 30$  mV (Figure 2c). This is likely because the  $\text{Na}^+$  counter-ions to the citrate are now trapped within the solvated PNIPAM, which resets the hydrodynamic slip surface, as well as due to the PNIPAM displacing citrate from the AuNP surface. The  $\text{NH}_2$ -PNIPAM shows even less net charge (around half as much as  $-\text{SH}$ ), presumably because the positively charged amines also neutralize the citrate. It appears that this reduced net charge is instrumental in allowing the Au cores to approach each other more closely, as well as in assembling larger overall aggregates. One possibility is the different net charge controls different thicknesses of additional PNIPAM to build up round each NP in the hot state, thus affecting the NP gap spacing (even though when

cold, the solvated coated NPs are all of similar size, Figure 2d). However, in this case, we expect screening from the more positive  $-\text{NH}_2$  facilitates thicker coatings and larger gaps, which is the opposite of that observed.

The only alternative is that even after coagulation, the AuNPs are able to move inside the sheath of PNIPAM (Figure 1, migration). The particles can then move closer together when coated by the more screened  $\text{NH}_2$ -PNIPAM if it has low enough  $M_w$ . Scanning electron microscope images (SEMs, Figure 2e,f) for aggregates which are dried when hot onto Si substrates to preserve their morphology, show larger sizes for  $-\text{NH}_2$  termination, and some evidence for the migration of AuNPs into the center of the aggregate via this mobility (Figure S2, Supporting Information). We note that the aggregates do not form fractals as expected in the diffusion-limited growth regime,<sup>[16]</sup> but adopt a near close-packed arrangement, which requires a net attractive force between the particles that is not so strong as to be irreversible (in other words, the particles retain mobility even when their minimum separation is reached). Because these aggregates are compact, there is limited charge screening possible, and thus they grow more slowly once the potential barrier for addition of one extra coated NP is greater than the thermal energy. All these features suggest that electrostatics is important for the particles within the collapsed polymeric network. We thus expect additional salt in solution to provide strong effects.

### 3.2. Charge Matters

Having now identified the significant role of charge in this reversible nanoassembly, we show that the results for amine termination can also be replicated with other functionalities when appropriate screening is provided. Introducing  $\geq 50 \times 10^{-3}$  M of NaCl produces strong redshifts for all functionalities of PNIPAM tested including also the negatively charged  $-\text{COOH}$  end group (Figure 3, Table 1). Without NaCl, only the  $-\text{NH}_2$  PNIPAM induces strong redshifts, however, the presence of NaCl gives redshifts exceeding  $\Delta\lambda > 100$  nm, with aggregates all exceeding 450 nm hydrodynamic diameter (thus containing  $>6000$  coated NPs, assuming there is no significant extra layer of PNIPAM surrounding each aggregate). At  $50 \times 10^{-3}$  M, the magnitude of the redshift depends on the functional termination of the PNIPAM, with  $\text{NH}_2 > \text{COOH} > \text{SH} \approx \text{bare}$ . Generally, salt decreases the zeta-potential of the coated NPs (Table S1, Supporting Information). With NaCl, the DLS hydrodynamic sizes are increased by up to 2-fold (Table 1). Given that the well-solvated chains should extend a distance  $L = N a \sigma^{1/3}$  for  $N$  units of the PNIPAM backbone of spacing  $a$ , with typical close-packed surface density

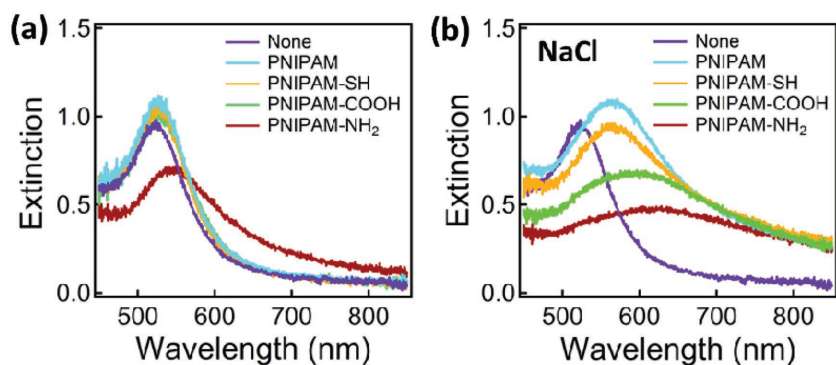


**Figure 3.** UV-vis extinction spectra of ANTs using different functionalized PNIPAM as indicated, both a) without, and b) with  $50 \times 10^{-3}$  M NaCl.

$\sigma \approx 0.3$ ,<sup>[17,18]</sup> then for terminations of  $-\text{NH}_2$ ,  $-\text{COOH}$ , we estimate  $L \approx 23$  nm and for  $-\text{SH}$ ,  $-\text{bare}$  PNIPAM, we predict  $L \approx 62$  nm (note the different molecular weights in Table 1). These are indeed similar to the coating thicknesses obtained from the DLS. This suggests that dense attachment of low  $M_w$  PNIPAM to these AuNPs is achieved (the Flory radius would imply surface densities  $\sigma^{1/3} \approx N^{-0.4} \approx 0.21$  and 0.14, respectively,<sup>[17]</sup> reducing  $L$  below that observed). Normally, the swelling ratio for such high density PNIPAM brushes is around  $\alpha \approx 3$ ,<sup>[18]</sup> which would imply that the collapsed-state gaps between AuNPs would be  $d = 2L/\alpha > 20$  nm, far larger than either directly observed (Figure 2e,f) or consistent with the spectra (Figure 3), as we discuss below. On the other hand, at lower surface densities, swelling ratios of  $\alpha \approx 11$  are found which would predict gaps of 7.1 nm ( $-\text{bare}$ ), 5.4 nm ( $-\text{NH}_2$ ), 9.5 nm ( $-\text{SH}$ ), and 4 nm ( $-\text{COOH}$ ), which should be directly compared with experiment. However, to understand the combined effect of both these gaps and of the different aggregate sizes on the plasmon resonance, requires detailed simulations of the optical response.

### 3.3. Calculations

Transfer Matrix (T-matrix) simulations are thus performed for ANT random close-packed aggregates of varying interparticle distance and aggregate size (Figure 4). Fixing the interparticle spacing of the NPs to 1 nm and increasing the size of the ANT cluster results in a redshift of the extinction peak (Figure 4a). This approximately linear response (Figure 4b) is similar to redshifts observed on a plasmonic chain with increasing numbers of particles.<sup>[19]</sup> Similarly, decreasing the interparticle distance of NPs in the cluster induces a significant redshift (Figure 4c,d). Unfortunately, the heavy computational resources required for these exact simulations (already with  $>600$  NPs) mean that interpolation has to be used for the largest aggregate sizes (see Section 2, Supporting Information). This predicts that

for  $-\text{NH}_2$  aggregates of 460 nm diameter and 5.4 nm gap (as extracted from the DLS above), a 55 nm spectral redshift should be obtained, which is much less than the 105 nm seen (Table 2). In order to provide a shift of this magnitude, the gaps between the AuNPs must be below 2.5 nm, which is half that predicted from the contraction of the coatings around individual NPs. Similar estimates can be made for the other PNIPAM terminations (Table 2).

While the actual gaps measured optically show larger contraction than expected for  $-\text{NH}_2$  (roughly half the predicted spacing), the gaps are roughly as expected for  $-\text{SH}$ ,  $-\text{COOH}$ , and  $-\text{bare}$  PNIPAM. To explain why  $-\text{NH}_2$  termination can access smaller

gaps, we consider the effect of AuNPs diffusing inside the aggregating halo of PNIPAM. These NPs can squeeze out polymer from within the gaps as long as charge repulsion between the Au cores is small enough. Since the  $-\text{NH}_2$  partially compensates the negative citrate charge, it can indeed reduce the repulsion between AuNPs and allow them to approach more closely (enhanced by their Van der Waals attraction). We note that little is known about the Debye screening length around a nanoparticle within a dense PNIPAM brush, although in solution for  $50 \times 10^{-3}$  M NaCl this Debye length is  $\approx 1.3$  nm outside the PNIPAM brush.

The main contribution of NaCl in this system is to reduce the screening length (and possibly also to increase the swelling ratio), demonstrating how the total redshift of the plasmon resonances is governed by electrostatics. The reduction in net

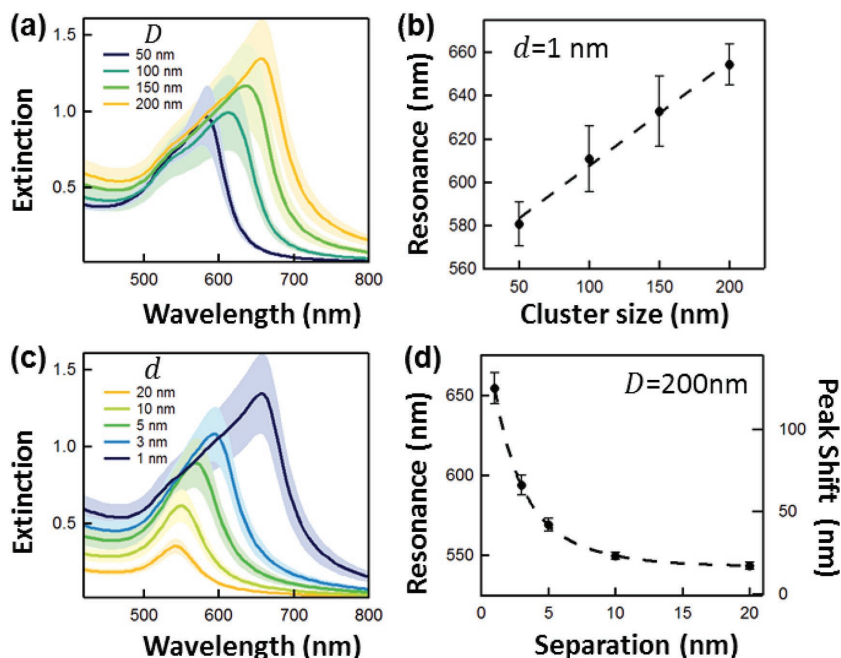


**Figure 4.** Simulated T-matrix optical response when a,b) changing aggregate diameter for 1 nm gaps, and c,d) changing separation between 16 nm AuNPs inside the aggregate of 200 nm diameter. AuNP diameter is 16 nm. Shaded areas correspond to results illuminating many specific close-packed random aggregate from different directions, averaged to give the solid line.

**Table 2.** Gap sizes and plasmon shifts ( $\Delta\lambda$ ) of the hybrid plasmonic system using PNIPAM with different termination groups.

Sample <sup>a)</sup>	–Bare	–NH <sub>2</sub>	–SH	–COOH
DLS predicted gap (nm)	7.1	5.4	9.5	4.0
DLS predicted $\Delta\lambda$ (nm)	47	55	42	70
Measured $\Delta\lambda$ (nm)	47	105	53	73
Plasmon gap estimated (nm)	7.1	2.5	7.3	3.8

<sup>a)</sup>Hydrodynamic diameter when cold (in presence of  $50 \times 10^{-3}$  M NaCl) provides estimate of PNIPAM solvated thickness, assumed to collapse by factor  $\alpha = 11$ . Together with the measured DLS aggregate diameter (Table 1), this predicts the plasmon redshifts that should be observed, which are compared with the observed redshifts. For comparison, the predicted average plasmonic gap between NPs is given, using the DLS size and measured plasmonic peak in the optical measurements.

charge on the Au cores allows them to approach more closely, while also allowing the cluster size to grow larger which produces  $\Delta\lambda > 100$  nm strongly redshifted resonances even for such small AuNPs. The addition of NaCl may also modify the hydrophobic interactions on the PNIPAM chains.<sup>[20,21]</sup> To study this, the concentration dependence with NaCl and the effect of different salts through the Hofmeister sequence are measured for PNIPAM–SH and bare-PNIPAM. As expected from the Debye length, increasing concentrations of NaCl progressively increase the redshift, which eventually saturates at 45 nm (Figure S3b, Supporting Information). However, the redshifts obtained are little influenced for either PNIPAM by adding ions of different Hofmeister strength (Figure S4, Supporting Information), suggesting this is not a factor here.

### 3.4. Role of Excess PNIPAM

With this qualitative understanding of the mechanisms involved in aggregate formation for PNIPAM of different functionalities and their resulting spectral redshifts, an outstanding question remaining is the need for an excess of free unbound PNIPAM.<sup>[13,14]</sup> Even for –NH<sub>2</sub>-terminated PNIPAM, there is an optimum concentration of  $20 \times 10^{-6}$  M and a reduced redshift either side (Figure S3d, Supporting Information). A reliance on excess PNIPAM in the actuation mechanism is highly undesirable as a self-contained system is preferential for all color-change devices or nanomachine applications (in biomedical applications excess PNIPAM will be unavailable).<sup>[9]</sup> Using AuNP@PNIPAM–SH (Figure 5), we show that excess PNIPAM leads merely to excess scattering when hot, while when salt is present, no excess PNIPAM is required to get

switching (Figure 5c). This observation shows that actuation in a self-contained “nanomachine” should be attainable using the LCST of PNIPAM. Moreover, it also suggests this system is a promising candidate for in vivo applications as it matches the biological fluid conditions where NaCl concentrations are normally around 0.1 M.

## 4. Conclusion

In summary, the evidence presented here leads to the conclusion that it is mainly the surface charge of AuNPs within PNIPAM, which determines whether they can aggregate or not. We establish that the main role of the amine functionality is in screening the charge of residual citrate groups that remain trapped postfunctionalization. The repulsion from these charges seems to dominate the magnitude of the redshift of ANTs in the collapsed state, with resulting gaps down to <3 nm giving strong plasmonic coupling. The effect of the amine-functionalized PNIPAM can be reproduced with other types of PNIPAM provided the surface NP charge is screened by other means, such as increasing the ionic strength of the solution. Our observations suggest that even in the collapsed gel state, the particles inside the clusters retain some mobility and are able to rearrange to adopt the minimal thermodynamically stable close-packed state. Finally, excess unbound PNIPAM is shown to be not crucial to the aggregation mechanism as was

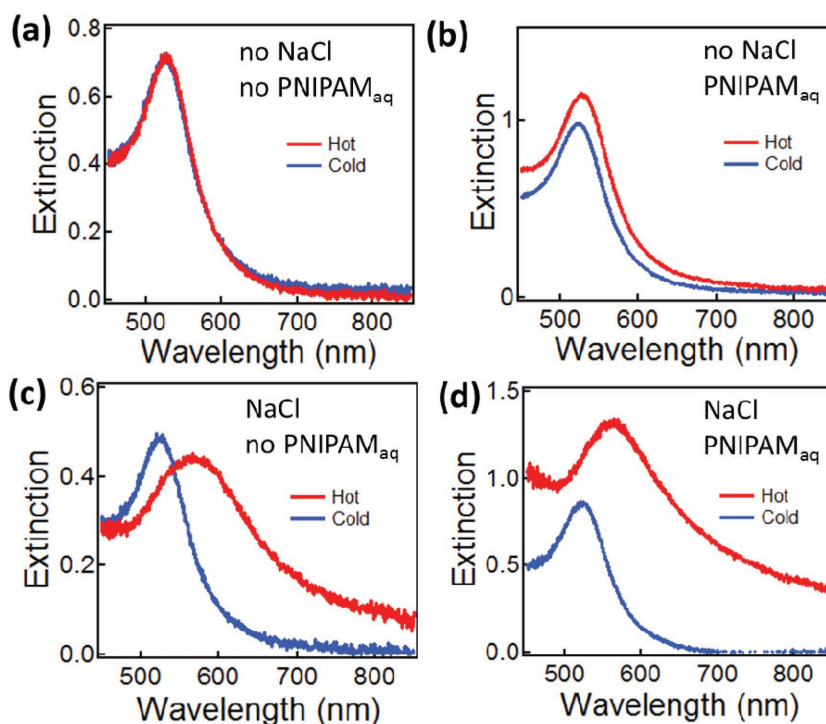


**Figure 5.** Optical response of ANTs using PNIPAM–SH under various conditions. a) In the absence of NaCl and with no free excess of PNIPAM<sub>aq</sub> (removed by repeated centrifugation),  $\Delta\lambda \approx 0$ . b) With excess PNIPAM<sub>aq</sub> but no NaCl,  $\Delta\lambda \approx 0$  but scattering increases from aggregating PNIPAM<sub>aq</sub>. c) In  $50 \times 10^{-3}$  M NaCl without excess PNIPAM<sub>aq</sub>, only the redshift is retained indicating that actuation is not dependent on excess PNIPAM<sub>aq</sub>. d) Excess PNIPAM<sub>aq</sub> and  $50 \times 10^{-3}$  M NaCl produces both a redshift and increased scattering.

previously suggested,<sup>[13,14]</sup> but is in fact only relevant if the electrostatic repulsion from the functionalized particles remains long range. These findings should enable the intelligent design of fast fully-reversible color-changing devices and actuating nanomachines with externally controlled stimuli.

## 5. Experimental Section

**Synthesis and Characterizations:** The 16 nm citrate-stabilized AuNPs were synthesized according to previous protocols.<sup>[22]</sup> Typically, HAuCl<sub>4</sub> solution (0.086 mg mL<sup>-1</sup>) was preheated to 100 °C, followed by rapid addition of 0.2 mg mL<sup>-1</sup> of sodium citrate solution. Within 20 min, the color of solution turned from light yellow to dark brown and eventually to pink red indicating formation of AuNPs. The residual sodium citrate ion concentration was estimated to be  $\approx 2 \times 10^{-3}$  M (much smaller than the salt concentrations subsequently added). The PNIPAM-NH<sub>2</sub> ( $M_w = 5.5$ k), PNIPAM-COOH ( $M_w = 5$ k), and PNIPAM ( $M_w = 10$ k) were obtained from Sigma Aldrich. The PNIPAM-SH (15k) was synthesized according to a previous report.<sup>[13]</sup> The LCST of these polymers was determined to be  $32 \pm 0.5$  °C. To prepare the solution of Au-PNIPAM, 1 mL of as-synthesized 16 nm AuNPs was mixed with 50  $\mu$ L PNIPAM solution (0.1 mg mL<sup>-1</sup>). Removal of excess PNIPAM was achieved with repeated centrifugation (12k rpm, 10 min) for three times. Extinction spectra were measured with an optical fiber spectrometer (USB2000, Ocean Optics). Hydrodynamic size and zeta-potential of the AuNP/PNIPAM hybrid colloidal system were measured via Zetasizer (Malvern). SEM images of the dried Au/PNIPAM clusters were captured with a LEO 1530VP (Zeiss).

**Theoretical Modeling:** The extinction cross-sections of ANT clusters were calculated using Mackowski's Multiple Sphere T-Matrix (MSTM, v3.0) code (available open source).<sup>[23]</sup> The calculations used randomly grown 16 nm gold nanoparticle cluster structures with defined cluster sizes and interparticle spacings. The algorithm for generating the clusters consisted of first adding a new AuNP onto the surface of the cluster from a randomized position and direction, and then allowing the new particle to relax to the nearest surface dimer at the specified interparticle distance (thus touching at least two other NPs). The cluster is grown using this method until a specified total diameter is reached. Over the size range of the clusters calculated, this method approximated the random diffusive growth of the cluster in the reaction-limited aggregation regime (i.e. without fractal aggregate generation). This was appropriate for the ANT clusters, since fractal configurations were not observed experimentally, which was believed due to the AuNP mobility within the clusters. The randomly grown AuNP clusters were then fully encased in a spherical hot PNIPAM medium ( $n = 1.42$ ) and surrounded with an external medium of water ( $n = 1.33$ ). The dielectric function of the AuNPs was interpolated from Johnson and Christy.

## Supporting Information

Supporting Information is available from the Wiley Online Library or from the author. Source data can be found at: <https://doi.org/10.17863/CAM.20243>.

## Acknowledgements

The authors acknowledge the support from EPSRC grants EP/G060649/1 and EP/L027151/1, ERC grant LINASS 320503, and Leverhulme Trust (ECF2016-606). Dr. T.D. thanks the support from 1000-talents Youth Program and start-up grant from Wuhan University. B.S. is grateful for the Talent Hub Program, Grant Agreement 291780. S.C. is grateful for the support from the Winton Programme for the Physics of Sustainability.

## Conflict of Interest

The authors declare no conflict of interest.

## Keywords

nanoparticle aggregation, plasmon resonance, PNIPAM, self-assembly, thermoresponsive polymers

Received: November 23, 2017

Revised: January 17, 2018

Published online:

- [1] A. Klinkova, R. M. Choueiri, E. Kumacheva, *Chem. Soc. Rev.* **2014**, *43*, 3976.
- [2] B. Gao, M. J. Rozin, A. R. Tao, *Nanoscale* **2013**, *5*, 5677.
- [3] L. Chen, H.-A. Klok, *Soft Matter* **2013**, *9*, 10678.
- [4] Y. Liu, X. Dai, S. Mallawaarachchi, H. Hapuarachchi, Q. Shi, D. Dong, S. H. Thang, M. Premaratne, W. Cheng, *J. Mater. Chem. C* **2017**, *5*, 10926.
- [5] S. Maji, B. Cesur, Z. Zhang, B. G. De Geest, R. Hoogenboom, *Polym. Chem.* **2016**, *7*, 1705.
- [6] M. I. Gibson, R. K. O'Reilly, *Chem. Soc. Rev.* **2013**, *42*, 7204.
- [7] D. Fava, M. A. Winnik, E. Kumacheva, *Chem. Commun.* **2009**, *0*, 2571.
- [8] M.-Q. Zhu, L.-Q. Wang, G. J. Exarhos, A. D. Q. Li, *J. Am. Chem. Soc.* **2004**, *126*, 2656.
- [9] T. Ding, V. K. Valev, A. R. Salmon, C. J. Forman, S. K. Smoukov, O. A. Scherman, D. Frenkel, J. J. Baumberg, *Proc. Natl. Acad. Sci. USA* **2016**, *113*, 5503.
- [10] R. Contreras-Cáceres, J. Pacifico, I. Pastoriza-Santos, J. Pérez-Juste, A. Fernández-Barbero, L. M. Liz-Marzán, *Adv. Funct. Mater.* **2009**, *19*, 3070.
- [11] S. Murphy, S. Jaber, C. Ritchie, M. Karg, P. Mulvaney, *Langmuir* **2016**, *32*, 12497.
- [12] Z. Qian, K. N. Guye, D. J. Masiello, D. S. Ginger, *J. Phys. Chem. B* **2017**, *121*, 1092.
- [13] S. T. Jones, Z. Walsh-Korb, S. J. Barrow, S. L. Henderson, J. del Barrio, O. A. Scherman, *ACS Nano* **2016**, *10*, 3158.
- [14] F. Han, A. H. Soeriyadi, S. R. C. Vivekchand, J. J. Gooding, *ACS Macro Lett.* **2016**, *5*, 626.
- [15] K. Kubota, K. Hamano, N. Kuwahara, S. Fujishige, I. Ando, *Polym. J.* **1990**, *22*, 1051.
- [16] R. W. Taylor, T.-C. Lee, O. A. Scherman, R. Esteban, J. Aizpurua, F. M. Huang, J. J. Baumberg, S. Mahajan, *ACS Nano* **2011**, *5*, 3878.
- [17] P. G. de Gennes, *Macromolecules* **1980**, *13*, 1069.
- [18] S. Varma, L. Bureau, D. Débarre, *Langmuir* **2016**, *32*, 3152.
- [19] R. Esteban, R. W. Taylor, J. J. Baumberg, J. Aizpurua, *Langmuir* **2012**, *28*, 8881.
- [20] Z. Zhang, S. Maji, A. B. d. F. Antunes, R. De Rycke, Q. Zhang, R. Hoogenboom, B. G. De Geest, *Chem. Mater.* **2013**, *25*, 4297.
- [21] Y. Zhang, S. Furry, D. E. Bergbreiter, P. S. Cremer, *J. Am. Chem. Soc.* **2005**, *127*, 14505.
- [22] J. Turkevich, P. C. Stevenson, J. Hillier, *J. Phys. Chem.* **1953**, *57*, 670.
- [23] D. W. Mackowski, M. I. Mishchenko, *J. Quant. Spectrosc. Radiat. Transfer* **2011**, *112*, 2182.